Coiling of Elastic Ropes

M. Habibi,[1,2] N. M. Ribe,[3] and Daniel Bonn[2,4]

[1]*Institute for Advanced Studies in Basic Sciences, Zanjan 45195-1159, Iran*
[2]*Laboratoire de Physique Statistique, École Normale Supérieure, 24, rue Lhomond, 75231 Paris Cedex 05, France*
[3]*Institut de Physique du Globe de Paris and Université de Paris-7, CNRS, Tour 14, 2, place Jussieu, 75005 Paris, France*
[4]*Van der Waals-Zeeman Institute, University of Amsterdam, Valckenierstraat 65, 1018 XE Amsterdam, the Netherlands*

(Received 13 April 2007; published 11 October 2007)

A rope falling onto a solid surface typically forms a series of regular coils. Here, we study this phenomenon using laboratory experiments (with cotton threads and softened spaghetti) and an asymptotic ''slender-rope'' numerical model. The excellent agreement between the two with no adjustable parameters allows us to determine a complete phase diagram for elastic coiling comprising three basic regimes involving different force balances (elastic, gravitational, and inertial) together with resonant ''whirling string'' and ''whirling shaft'' eigenmodes in the inertial regime.

DOI: 10.1103/PhysRevLett.99.154302 PACS numbers: 46.32.+x, 46.70.Hg

All mountaineers know that a rope held vertically and dropped onto a surface will often coil spontaneously. The initial stage of the coiling is just the buckling of the rope under its own weight. In general, when a solid material buckles, the subsequent nonlinear evolution of the instability can occur in two ways. If the material is very stiff, it will break. If however it is sufficiently flexible, the structure will undergo a large finite-amplitude deformation whose dynamics are essentially nonlinear. In many cases, the nonlinearity is due to the breakdown at large strain of an initially linear relation between stress and displacement, either because the quadratic terms in the elastic strain tensor [1] become significant or because the material no longer satisfies Hooke's law. Much progress has been made recently in understanding these sorts of nonlinear behavior in structures such as crumpled sheets of paper [2,3] and crumpled wires [4]. However, nonlinear behavior can also occur even in a linearly elastic material if the final deformed shape of the structure is far from the initial state. The classic example of such ''geometrical'' nonlinearity is the large deformation of elastic rods described by the Kirchhoff equations [5], examples of which include the kinking of telephone cables on the ocean floor [6], handedness reversal in the coiled tendrils of climbing plants [7], the supercoiling of DNA strands [8], and the steady rope coiling that we study here.

Much work has been done recently on the analogous phenomenon of the coiling of a ''liquid rope'' such as a thread of honey falling onto toast. Experimental and theoretical studies [9–15] have revealed a remarkable dynamical richness in this instability, which exhibits four different regimes depending on the relative importance of viscous forces, gravity, and inertia, as well as multistable behavior in a range of fall heights. By contrast, elastic rope coiling has to our knowledge never been studied experimentally. The sole theoretical investigation known to us is [16], who solved numerically a set of Kirchhoff-type equations for a steadily coiling rope and correctly identified the two regimes that involve no inertia. However, the inertial terms in the equations of [16] all have the wrong sign, and so the corresponding numerical solutions are incorrect.

In this Letter, we present the first experiments on elastic rope coiling together with a detailed numerical study. The two agree remarkably well without any adjustable parameter, allowing us to determine a complete phase diagram for coiling as a function of the fall height H and the feeding velocity U. We find a surprisingly complex dynamics involving three distinct regimes characterized by different force balances (elastic, gravitational, and inertial) as well as two sets of resonant modes within the inertial regime.

Experimental procedure.—We used two different experimental setups to observe coiling over wide ranges of values of H and U. In the first setup, ordinary rope or sewing thread was wound onto a wheel, which was then rotated by an electric motor to feed the rope down through a hole at a rate $U = 0.3$–$200\ \mathrm{cm\,s^{-1}}$ onto a glass plate or thick piece of paper 2–200 cm below. We eliminated preexisting curvature in the ropes either by ironing them or by wetting them with water and suspending them with a weight attached to the lower end. In a second setup, used for very low fall heights, pieces of spaghetti 24–26 cm long that had been presoftened in water were ejected downward from a vertical glass tube either using a syringe (for higher values of U) or by pushing with a rod (for lower U).

The physical properties of the ropes used are listed in Table I. The diameter d was measured with a digital vernier. The mass per unit length λ was measured by weighing a given length of rope. The Young's modulus E was determined by measuring (to within 0.05 mm using a digital vernier) the downward deflection y of the free ends of horizontally clamped pieces of rope with different lengths L, and then using least-squares regression against the analytical prediction $y = 8\lambda g L^4/\pi E d^4$ of the linear theory of elastic rods [17] to infer E to within $\pm 20\%$. We verified that the deflection did not depend on the orientation of the rope about its axis, implying that natural curvature had been successfully eliminated.

TABLE I. Physical properties of experimental ropes.

Rope	Composition	d (mm)	λ (kg m^{-1})	E (Pa)
1	Polyester thread	1.5	3.0×10^{-4}	1.5×10^{5}
2	Cotton thread	0.5	1.1×10^{-4}	2.9×10^{6}
3	Cotton thread	0.5	1.1×10^{-4}	1.5×10^{7}
4	Thick cotton thread	1.0	2.4×10^{-4}	8.2×10^{5}
5	Cotton thread	0.75	2.9×10^{-3}	8.5×10^{6}
6	Spaghetti no. 5	1.7	2.7×10^{-3}	6.9×10^{5}
7	Spaghetti no. 7	2.5	6×10^{-3}	5.2×10^{4}

We measured U by frame counting on movies taken with a webcam (≤ 15 frames s^{-1}) or a rapid CCD camera (≤ 1000 frames s^{-1}). The coil radius R was measured (to within 0.2 mm) either with a vernier or by counting pixels on photographs. Small fall heights H were measured to within 0.2 mm from photographs, and larger heights to within 1 mm using a ruler.

Experimental observations.—For most of the ropes listed in Table I, we performed a first series of experiments varying H with U fixed, and a second varying U with H fixed. Figure 1 shows some of the coiling configurations observed, and Fig. 2 shows a selection of experimental measurements of R as a function of H and U. Two different types of behavior are seen, depending on whether the coiling object is spaghetti fed from very low heights (≤ 1.3 cm in Fig. 2) or thread fed from a height of at least several cm. For the spaghetti [Fig. 1(a); open squares in Fig. 2], R increases with H [Fig. 2(a)] but is independent of U [Fig. 2(b)]. For threads, R also increases with height [Fig. 2(a), circles and solid squares]. However, the dependence on U is more complicated: R is first nearly independent of U, then increases, then decreases by a factor ≈ 2, and finally increases again [Fig. 2(b), open and solid circles]. Moreover, at high feeding velocities, the thread sometimes becomes unstable to an unsteady "figure of eight" mode [Fig. 1(c)] that can persist as long as the length of the thread permits, in contrast to the transient nature of such patterns in liquid rope coiling [13,15].

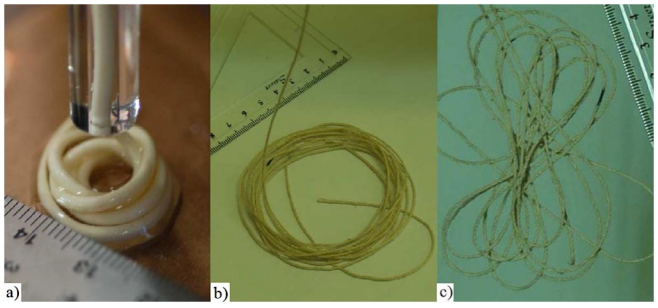

FIG. 1 (color online). Typical coiling configurations for ropes whose physical properties are listed in Table I. The numbers on the scale in each panel indicate cm. (a) rope 5, $H = 1.2$ cm, $U = 26$ cm s^{-1}; (b) rope 4, $H = 30$ cm, $U = 2.3$ cm s^{-1}; (c) rope 4, $H = 80$ cm, $U = 100$ cm s^{-1}.

Slender-rope model.—The diversity of behavior shown in Fig. 2 can be understood with the help of a numerical model for the motion under gravity of a slender elastic rope with inertia. As noted by [16], coiling is steady when viewed from a reference frame that rotates with the angular velocity $\boldsymbol{\Omega}$ of the rope's contact point with the surface. The equations we used to describe coiling in this frame are those of [16], but with the correct signs of the centrifugal acceleration $\boldsymbol{\Omega} \times (\boldsymbol{\Omega} \times \boldsymbol{x})$, the Coriolis acceleration $2\boldsymbol{\Omega} \times \boldsymbol{U}$, and the acceleration $U\boldsymbol{U}'$ in the corotating frame, where $\boldsymbol{x}(s)$ is the position of the rope's axis as a function of arclength s along it, $\boldsymbol{U} = U\boldsymbol{d}_3$, $\boldsymbol{d}_3(s) \equiv \boldsymbol{x}'$ is the unit vector tangent to the axis, and primes denote d/ds. We also used a corrected expression $I = \pi d^4/64$ for the moment of inertia of the rope's cross-section about a diameter. The model equations involve 12 dependent variables: $\boldsymbol{x}(s)$ (3 components); four Euler parameters that describe the orientation of a local basis comprising $\boldsymbol{d}_3$ and two material unit vectors $\boldsymbol{d}_1(s)$ and $\boldsymbol{d}_2(s)$ normal to the axis; the curvatures of the axis about $\boldsymbol{d}_1$ and $\boldsymbol{d}_2$, respectively; and the three components of the force acting on the rope's cross-section. The first-order ODEs satisfied by these variables comprise seven purely geometrical equations; three equations of global (integrated across the rope) force balance in the directions $\boldsymbol{d}_i$; and two equations of global torque balance about the directions $\boldsymbol{d}_1$ and $\boldsymbol{d}_2$. We solved the resulting

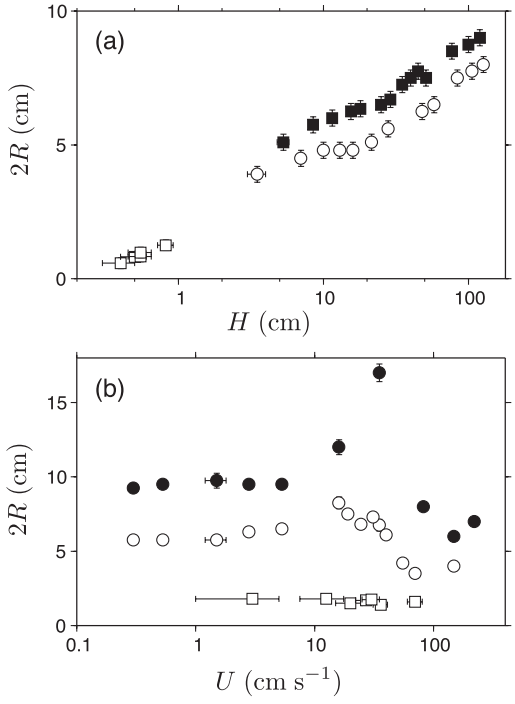

FIG. 2. Experimental measurements of the coil radius R. (a) R as a function of H for rope 6 with $U = 2$ cm s^{-1} (open squares), rope 1 with $U = 10$ cm s^{-1} (solid squares), and rope 2 with $U = 10$ cm s^{-1} (circles). (b) R as a function of U for rope 6 with $H = 1.3$ cm (squares), rope 5 with $H = 50$ cm (solid circles), and rope 2 with $H = 100$ cm (open circles).

twelfth-order two-point boundary-value problem numerically using the method of [16].

Because the numerics predict the existence of resonant eigenmodes (see below), we present the results in terms of the coiling frequency $\Omega \equiv U/R$ rather than the radius R. Nondimensionalization of the model equations shows that the dimensionless frequency $\hat{\Omega} \equiv \Omega(d^2E/\rho g^4)^{1/6}$ depends only on the dimensionless height $\hat{H} = H(\rho g/d^2E)^{1/3}$ and the dimensionless feeding velocity $\hat{U} = U(\rho/d^2g^2E)^{1/6}$. Figure 3 shows numerically calculated curves of $\hat{\Omega}(\hat{H})$ for several values of $\hat{U}$. Coiling can occur in three regimes, depending on how the elastic bending forces in the "coil" portion of the rope are balanced. Per unit rope length, the magnitudes of the elastic (E), gravitational (G), and inertial (I) forces are

$$F_E \sim Ed^4R^{-3} \qquad F_G \sim \rho g d^2, \qquad F_I \sim \rho d^2U^2R^{-1}. \tag{1}$$

In the first or "elastic" regime, both gravity and inertia are negligible (F_G, $F_I \ll F_E$) and the net elastic force acting on every element of the rope is zero. This corresponds to a standard situation in elasticity theory where the deformation of a rod is determined solely by the conditions imposed at its ends. A second, "gravitational" regime occurs

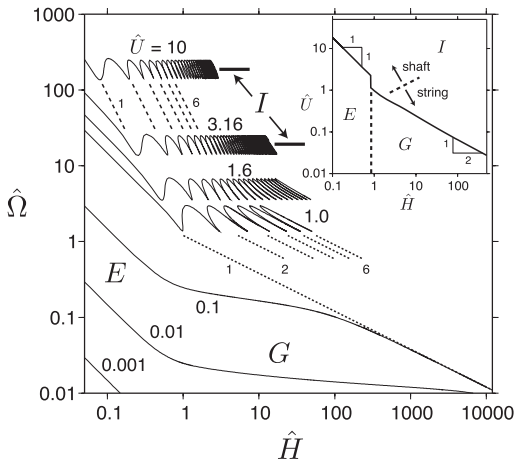

FIG. 3. Main portion: Dimensionless coiling frequency $\hat{\Omega} \equiv \Omega(d^2E/\rho g^4)^{1/6}$ as a function of dimensionless fall height $\hat{H} \equiv H(\rho g/d^2E)^{1/3}$ for several values of the dimensionless feeding velocity $\hat{U} = U(\rho/d^2g^2E)^{1/6}$. The curves for $\hat{U} \geq 1.0$ continue indefinitely to the right (not shown). Portions of the curves labeled E and G and the horizontal bars labeled I correspond to the frequencies (2). The first six "whirling string" and "whirling shaft" eigenfrequencies are indicated by dotted and dashed lines, respectively. Inset: Phase diagram for coiling as a function of $\hat{H}$ and $\hat{U}$. The frequency $\hat{\Omega}(\hat{H}, \hat{U})$ is multivalued everywhere above the solid line. The vertical dashed line indicates the smooth transition between elastic (E) and gravitational (G) coiling. The dashed line in the inertial (I) portion of the diagram indicates a smooth transition between whirling string and whirling shaft modes.

when inertia is negligible and the elastic forces are balanced by gravity ($F_G \approx F_V \gg F_I$). Finally, "inertial" coiling occurs when gravity is negligible and the elastic forces are balanced by inertia ($F_I \approx F_V \gg F_G$). The corresponding coiling frequencies Ω_E, Ω_G and Ω_I can be found by estimating R and then using the identity $\Omega = U/R$. For elastic coiling, $R \sim H$. For gravitational and inertial coiling, R is obtained from the force balances $F_G \approx F_E$ and $F_I \approx F_E$, respectively. The results are

$$\Omega_E \sim UH^{-1}, \qquad \Omega_G \sim U(\rho g/d^2E)^{1/3}, \qquad \Omega_I \sim U^2(\rho/d^2E)^{1/2}. \tag{2}$$

The scaling law for Ω_E corresponds to the portions of the curves with slope $= -1$ (labeled E) in the main part of Fig. 3, and that for Ω_G (equivalent to Eqn. 2.4 of [16]) corresponds to the nearly horizontal portions (labeled G). Ω_G also depends on H, but in a way that is too weak to be determined by scaling analysis. Finally, the scaling law for Ω_I corresponds to the horizontal lines labeled I.

Figure 3 reveals surprising complexity in the inertial regime, where $\hat{\Omega}(\hat{H})$ oscillates about the horizontal lines corresponding to Ω_I. This behavior reflects the presence of resonant eigenmodes in the nearly vertical upper portion ("tail") of the rope that are excited whenever one of its natural frequencies is close to the frequency Ω_I set by the coil at the bottom. These modes have two limiting forms. In the first limit, represented, e.g., by the rightmost portion of the curve $\hat{\Omega}(\hat{H})$ for $\hat{U} = 1.0$ in Fig. 3, the tail behaves as a steadily whirling "string" (i.e., a rope with negligible bending resistance) under gravity. Its eigenmodes are identical to those of a hanging chain, with eigenfrequencies Ω_n^{string} that satisfy $J_0(2\beta) = 0$, where $\beta = \Omega_n^{\text{string}}(H/g)^{1/2}$ and J_0 is the Bessel function of the first kind of order zero. The first six eigenfrequencies Ω_n^{string} are shown by the dotted lines with slope $-1/2$ in Fig. 3. For $n \geq 5$, these coincide closely with the segments of the curve $\hat{\Omega}(\hat{H})$ for $\hat{U} = 1.0$. The gravest ($n = 1$) whirling string mode is the limiting form of the G mode as $\hat{H} \to \infty$.

In the second limit, the tail behaves as a "whirling shaft" ([17], § 286) in which the centrifugal force is balanced by elastic bending forces. The lateral displacement $r(s)$ of the tail now satisfies $(Ed^2/16\rho)r'''' = \Omega^2 r$. Solving this subject to the end conditions $r(0) = r'(0) = 0$ (clamped) and $r''(H) = r'''(H) = 0$ (free), we find that the eigenfrequencies Ω_n^{shaft} satisfy $\cos p \cosh p = -1$, where $p^2 = 4H^2(\rho/d^2E)^{1/2}\Omega_n^{\text{shaft}}$. The first six of these eigenfrequencies are shown on Fig. 3 by dashed lines with slope -2. For $n \geq 5$, they align closely with the segments of the curves $\hat{\Omega}(\hat{H})$ for $\hat{U} = 3.16$ and 10.

The phase diagram implied by the curves $\hat{\Omega}(\hat{H}, \hat{U})$ appears as an inset in Fig. 3. The $(\hat{H}, \hat{U})$-plane is divided into three regions representing elastic (E), gravitational (G), and inertial (I) coiling. The inertial region in turn comprises two parts corresponding to "whirling string"

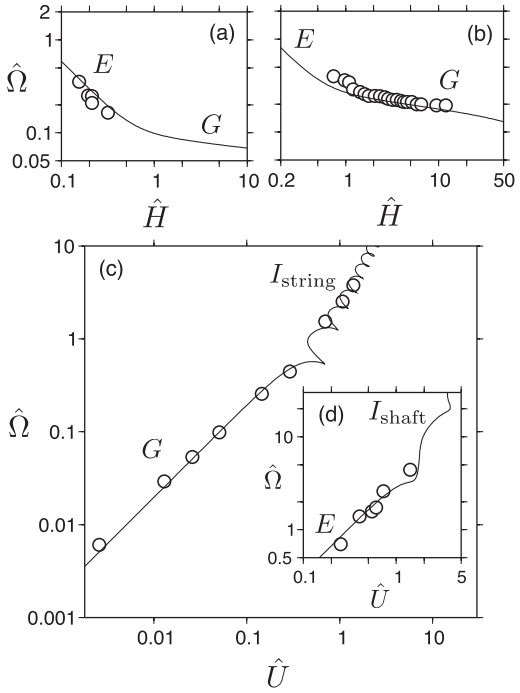

FIG. 4. Comparison of experimentally measured (circles) and numerically calculated (lines) coiling frequencies. The dimensionless frequency $\hat{\Omega}$, height $\hat{H}$, and feeding velocity $\hat{U}$ are defined in the text. The symbols E, G, and I indicate elastic, gravitational, and inertial coiling, respectively, and the subscripts "string" and "shaft" indicate the dominant resonant mode type in the portion of the inertial regime in question. Error bars (omitted) reflecting the composite errors of Ω, H, U, λ, d, and E rarely exceed twice the symbol size. (a) Rope 7 with $U = 2\ \mathrm{cm\,s^{-1}}$; (b) Rope 3 with $U = 10\ \mathrm{cm\,s^{-1}}$; (c) Rope 3 with $H = 30$ cm; (d) Rope 6 with $H = 1.3$ cm.

and "whirling shaft" resonant modes, with a smooth transition between them.

Comparison with experiment and with liquid rope coiling.—Figure 4 shows the dimensionless coiling frequencies measured in four series of experiments (circles), together with the predictions of the numerical model for the same values of H, U, d, λ, and E (lines.) Three regimes (E, G, and I_{string}) are clearly captured by the experiments, and the fourth (I_{shaft}) is represented by the topmost circle in Fig. 4(d). The excellent agreement between the numerics and the experiments with no adjustable parameters is strong evidence for the validity of the scaling laws and the phase diagram presented above. In terms of the original measurements of R vs. U [Fig. 2(b)], the constant radius at low U corresponds to the G regime, the subsequent increase to the transition between G and I coiling, and the final decrease to the I regime.

In closing, we compare the behavior of coiling elastic and liquid "ropes." An obvious difference is that a falling liquid rope is stretched by gravity so that its diameter decreases downward from the extrusion point. Allowing for this effect, however, one finds that liquid rope coiling has "viscous" and "gravitational" regimes that are exactly analogous to the elastic and gravitational coiling regimes, respectively, of an elastic rope [11,12]. Matters are more complicated if inertia is significant. Ribe *et al.* [13] showed experimentally and theoretically that liquid ropes can support "whirling string" resonant modes analogous to those documented here, but with eigenfrequencies modified by the rope's nonuniform diameter. By contrast, there is no experimental or numerical evidence that "whirling shaft" eigenmodes can exist on liquid ropes. But even the whirling string modes on a liquid rope disappear if the fall height is sufficiently great, at which point coiling occurs in a "pure" inertial regime identified by [10]. This regime has no equivalent in an elastic rope, for which the resonant modes seen in Fig. 3 appear to persist to arbitrarily large heights.

This work has been supported by Center for International Research and Collaboration (ISMO) and the French embassy in Tehran. We thank R. Golestanian and J. Lister for help, and three anonymous referees for careful reviews. LPS de l'ENS is UMR 8550 of the CNRS, associated with the Universities Paris 6 and 7. This is IPGP contribution No. 2290.

[1] L. D. Landau and E. M. Lifshitz, *Theory of Elasticity* (Pergamon Press, Oxford, 1959).
[2] M. BenAmar and Y. Pomeau, Proc. R. Soc. A **453**, 729 (1997).
[3] E. Sultan and A. Boudaoud, Phys. Rev. Lett. **96**, 136103 (2006).
[4] C. C. Donato, M. A. F. Gomes, and R. E. de Souza, Phys. Rev. E **67**, 026110 (2003).
[5] A. Goriely and M. Tabor, Nonlinear Dynamics **21**, 101 (2000).
[6] J. Coyne, IEEE Journal of Oceanic Engineering **15**, 72 (1990).
[7] A. Goriely and M. Tabor, Phys. Rev. Lett. **80**, 1564 (1998).
[8] A. Balaeff, C. R. Koudella, L. Mahadevan, and K. Schulten, Phil. Trans. R. Soc. A **362**, 1355 (2004).
[9] L. Mahadevan, W. S. Ryu, and A. D. T. Samuel, Nature (London) **392**, 140 (1998).
[10] L. Mahadevan, W. S. Ryu, and A. D. T. Samuel, Nature (London) **403**, 502 (2000).
[11] M. Maleki, M. Habibi, R. Golestanian, N. M. Ribe, and D. Bonn, Phys. Rev. Lett. **93**, 214502 (2004).
[12] N. M. Ribe, Proc. R. Soc. A **460**, 3223 (2004).
[13] N. M. Ribe, H. E. Huppert, M. Hallworth, M. Habibi, and D. Bonn, J. Fluid Mech. **555**, 275 (2006).
[14] N. M. Ribe, M. Habibi, and D. Bonn, Phys. Fluids **18**, 084102 (2006).
[15] M. Habibi, M. Maleki, R. Golestanian, N. Ribe, and D. Bonn, Phys. Rev. E **74**, 066306 (2006).
[16] L. Mahadevan and J. B. Keller, Proc. R. Soc. A **452**, 1679 (1996).
[17] A. E. H. Love, *A Treatise on the Mathematical Theory of Elasticity* (Dover, New York, 1944).